CHAPTER–3B

Photophysical Properties of Bis(pyrenyl)-di-imine: Aggregation Induced Emission on Tuning the Spacer Group from Phenylene to Alkylene

Photophysical Properties of Bis(pyrenyl)-di-imine: Aggregation Induced Emission on Tuning the Spacer Group from Phenylene to Alkylene

3B.1 Introduction

In chapter 3A, relation between solid-state arrangement and photophysical properties of bis(aryl)-alkylene-di-imines has been discussed. The current chapter deals with a faint fluorescent pyrene molecular system which is introduced as bis(pyrenyl)-di-imine and the spacer group of such compounds is varied from phenylene to alkylene (Scheme 3B.1). In general, a fluorescent organic molecule involves a large π-conjugated system of polycyclic aromatic rings[1] and are promising candidates for providing intense structured emission bands with high quantum yields. The major drawback in designing organic materials based on polycyclic aromatic system is the aggregation caused quenching (ACQ)[2] which limits their use in practical applications such as OLED, where the materials are required in the solid-state. In chapter 3A, effect of alkylene chain length on aggregation induced emission (AIE) and photoluminescence property of different molecular systems have been discussed.[3] AIE results when the molecules in aggregated state undergo conformational changes which restrict free rotations/vibrations and also prevent π-π stacking interactions thereby inhibiting the non-radiative decays. Hence, aggregation in such compounds will result in photoluminescence. There has been an enormous increase in the research focus on the materials possessing AIE properties.[4] The term AIE was coined[5] and this field was explored[6] by the Tang and co-workers. Later on, Z.G. Shuai, Curtias,[7] Xutang Tao,[8] Inamur Laskar,[9] Suresh Das,[10] Shengyu Feng,[11] Xiangge Zhou,[12] Kazuo Tanaka,[13] Zhen Li,[14] Aurelie Perrier,[2a] Zhong chen,[15] Lili Lin,[2b] etc., and their co-workers have been vigorously involved in the research activities in this field. The recent review paper on AIE by Wang and co-workers elaborately describes the pioneering research activities undertaken by various groups and highlighted the synthesized AIE materials along with their applications.[16]

Many explanations have been provided to decode the AIE effect, which include restriction of intramolecular rotation in the aggregates/solid states, formation of J-aggregates, intramolecular planarization, restriction of intramolecular charge transfer and twisted intramolecular charge transfer.[17] To understand the structure-property relationship properly, there is still requirement for elucidating the AIE from the view point of supramolecular structure and molecular packing via various noncovalent interactions. Systematic crystal structure analysis of the compounds along with their solid-state photophysical data will lead to classify the AIE properties arising

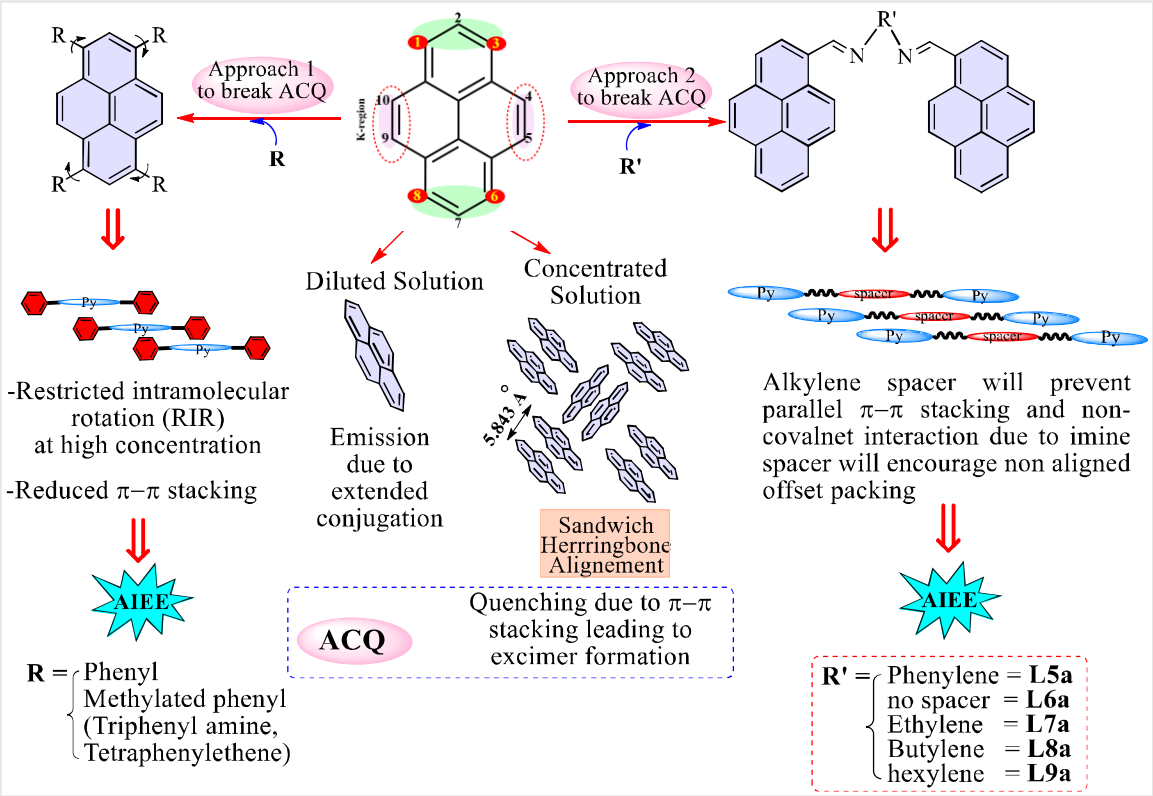

Scheme 3B.1: Approaches to remove thorny ACQ effect of pyrene[18]

due to planarization, J-aggregation, and so on. This will give us an idea about how the non-covalent interactions in the aggregates/solid states force the molecules to attain a geometry responsible for generating a specific photophysical property.

Polyatomic hydrocarbons (PAHs) like pyran, fluorene, coumarin, carbazole, phenothiazine, pyrene etc., have been explored widely for fluorescence applications.[19] I. B. Berlman has studied the photophysical properties of PAHs and established the correlation between the 'nuclear conformation' and 'fluorescence and absorption' characteristics of the compounds. It was concluded that planar geometry in ground state and excited state are more susceptible to form excimer/quenching than non-planar geometry.[20] Pyrene, known as the family of blue emitter because of the intrinsic extension of π-conjugation, is explored by several groups to synthesise blue emitting materials with adequate performance. Moorthy and co-workers have reported sterically hindered tetraarylpyrene as blue emitter in OLEDs.[21] Akiyama et al., have used tetraphenylpyrene as layer in OLED structure for field effect transistor.[22] Functionalized pyrene has been extensively used as a fluorophores for fluorescence, optical, electrical and bio engineering because of their photoluminescence properties, polarity, extended conjugation system, structural planarity and chemical stability.[23] Li et al., have categorised the molecular

packing of aromatic hydrocarbon in their review article, where pyrene molecules formed a sandwich herringbone alignment with minimum 5.843 Å distances (Scheme 3B.1).[14] Cheng and co-workers introduced a phenylene ring into two pyrene moieties and resulted in a the structure with twisted geometry which led to low degree of aggregation and in turn showed higher quantum yield than typical pyrene excimer emission.[18] Pyrene molecules due to planar geometry will always have a tendency of excimer formation in higher concentration, which in turn will lead to the notorious effect of ACQ. Pyrene molecule gives emission in the range of 375-405 nm and a broad band appears at around 460 nm due to the excimer formation.[24] Functionalization of pyrene has given an enormous scope to derive favourable optical properties with high quantum yields in solid state by preventing ACQ. Theoretical studies have given favourable substitution positions in pyrene moiety which may lead in achieving good photophysical properties (Figure 3B.1).[25] Recently, 2,7-positions of pyrene core were substituted with tetraphenylethene (TPE) and triphenylethene (TP'E) by Tang group which affected the change from ACQ to AIE.[26] The above mentioned tetraarylpyrene, aryl groups were attached in 1,3,6,8 active positions. By changing the aryl moieties with hindered substituent supressed the face to face π-π stacking in better way.[21] Later on, Tang and co-workers observed diminishing ACQ effect in the 1,3,6,8-TPE substituted pyrene derivative, and the synthesized compound was used in LED and it showed excellent performance (quantum efficiency 4.95%).[27] Significantly, it has been observed that when the periphery of pyrene having substituents such as phenyl ring, methylated phenyl ring, triphenylamine (TPA) and (TPE), then aggregation induced enhanced emission (AIEE) is resulted in solid state.[21, 27] This type of attachment of AIE luminogens in peripheral could solve the thorny ACQ effect which is schematized in scheme 3B.1.

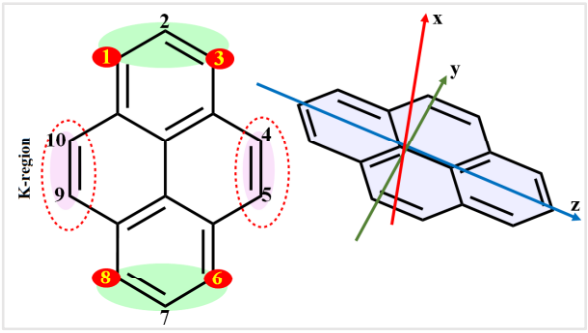

Figure 3B.1: Effective substitution positions in pyrene which may prevent ACQ**.** The red circles represent the more active position on the periphery of pyrene

The current chapter describes the luminescent properties of bis(pyrenyl)-di-imines, where it has been observed that AIE and ACQ are dependent on the chemical nature of the spacer group. Systematic analysis of crystal structure along with photophysical studies will lead to an understanding on the role of aryl groups and alkylene chain length present in spacer group of

the compounds in AIE properties. Our group has previously reported the photophysical properties of pyridyl based Schiff bases (bis(pyridyl)-alkylene-di-imine) and their crystal structure analysis to rationalize the effect of alkylene spacers on AIE properties which is described in chapter 3A.[28] The focus of the current study is to break the ACQ effect in pyrenes. One of strategies to minimize ACQ, as shown in scheme 3B.1, involves in decorating the ACQ luminogen pyrene with chemical functionalities, which may be capable of forming non-covalent interactions. Another strategy may involve inserting alkylene groups which will result in creating non-planar arrangements and thereby reducing the face-to-face stacking and hence the ACQ can be curtailed.

Feng et al., reviewed typical methodologies for the synthesis of pyrene functionalized luminescent materials.[29] They have discussed examples of the active sites of pyrene core, such as (1,3,6,8), K-region (4,5,9,10) and nodal plane (1,7). How these active regions are functionalised for suppressing the π-π stacking of pyrene rings also examined. Substitution at the K-region leads to interesting optical properties. Some examples where substituted pyrenes showed interesting photophysical properties include 4,5,9,10-tetrakis[(4-methoxy(phenyl)ethynyl]pyrene which emitted pure blue light at λ_{em} 453 nm.[30] Four, five-substituted pyrene-fused azaacenes, which showed emission at NIR region (λ_{em} 860 nm).[31]

Apart from the substitution of the pyrene at active sites, presence of functional groups with pyrene capable of forming non-covalent synthons were also explored by various research groups for generating light emitting properties.[18] Several groups have investigated pyrene-imine system which capable to forming non-covalent interactions.[32] Shellaiah et al., have worked on pyrene and anthracene-based Schiff base derivatives which showed turn on fluorescence sensing of Cu^{2+} and Fe^{3+} ions.[33] Babgil et al., have reported the optical sensing property of pyrene Schiff base in different acidic conditions.[34] Espinosa's group has used **L6a** as a receptor for sensing of Hg^{2+} and Cu^{2+} ions, where **L6a** showed quenched emission..[35] After binding the cations, complex formation prevented the quenching of **L6a** and deep pink emission with Cu^{2+} and green emission with Hg^{2+} were observed . Later, Martino et al., have also reported **L6a** as a sensor for Hg^{2+} and Cu^{2+} ions from absorption and emission spectra analysis.[36] The unique complexation (cations:**L6a**) was verified from the well-defined two isosbestic points for Hg^{2+} at 378 nm and 460 nm in UV-visible spectra. Here, L6a could be used to distinguish between Cu^{2+} and Hg^{2+}. Ganeshpandian's group[37] has synthesized a ruthenium complex of **L7a** for biological study, where it was observed that the luminescent

characteristics of pyrenyl group and extended aromatic ring system in **L7a** acted as a promising reagent for photo-active chemical nuclease. Kumar and co-workers presented **L7a** as a chemosensor for Hg^{+2} ion.[32a] After complex formation, the monomer (398 nm) and poor excimer (480 nm) emission of **L7a** enhanced due to the suppression of photoinduced electron transfer from imine nitrogen to the photoexcited pyrene moiety. The involvement of lone pairs of imine nitrogen in binding with Hg^{+2} confirmed from ^{1}H-NMR study.

In this chapter, effect of spacer group of bis(pyrenyl)-di-imines on the optical properties has been studied through correlating the structural features. A series of bis(pyrenyl)-di-imines molecules studied in the current chapter include compounds with varied the spacer group which ranges from alkylene to phenylene. The major discussion is based on the following points: (i) type of spacer capable of removing ACQ (ii) crystal structure analysis of **L5a** and rationalizing the photophysical behaviour based on its structural behaviour (iii) rigid verses flexible spacer in generating aggregates which in turn activate AIE.

3B.2 Experimental

3B.2.1 General

^{1}H and ^{13}C NMR spectra were recorded on a Bruker 400 MHZ spectrometer. FTIR spectra were obtained from Shimadzu IRAffinity-1S system. Powder X-Ray Diffraction (XRD) data was collected using a Rigaku miniflex II, λ =1.54 Å, Cu Kα. UV-Visible and fluorescence spectra were recorded on Jasco V-650 spectrophotometer and Fluorimax-4 0426C0809 respectively.

3B.2.2 Single Crystal XRD

The single-crystal XRD analysis of **L5a** was done at Narendrapur Ramkrishna Mission, Kolkata, using a Bruker AXS D8 QUEST ECO diffractometer equipped with monochromatic Mo-target rotating anode X-ray and graphite monochromator α radiation with λ = 0.71073 Å by ω and φ scan technique. The integrated diffraction data, unit cell, and data correction were performed using Bruker SAINT system, SMART, and SADABS respectively. The structure was solved by SHELXS-97 through the direct method and refined by full-matrix least-squares based on F^2 through SHELXS-2018/3.[38] The hydrogen atoms were added at determined positions as riding atoms and non-H atoms were refined anisotropically.

3B.2.3 Synthesis of (1*E*,1'*E*)-*N*,*N*'-(1,4-phenylene)bis(1-(pyren-1-yl)methanimine) (L5a)

p-Phenylene diamine (0.270 g, 2.5 mmol) dropwise and then catalytic amount of trifluoroacetic acid (TFA, 2-3 drops) were added to the solution of 1-pyrenecarboxaldehyde in dimethylacetamide (DMA) (1.15 g, 5 mmol). The mixture was refluxed for 24 hours. Bright yellow precipitate was removed by filtration and recrystallized from chloroform (Table 3B.1). Yield: 59%; Melting point: 255 - 256 ˚C; IR (cm^{-1}): 3047 (w), 2360 (w), 1597 (s), 1481 (m), 1203 (m), 964 (m), 895 (m), 849 (m), 763 (m), 710 (s), 610 (w), 502 (w) (Figure A-36); ^{1}H NMR (400MHz, DMSO-d_6) δ ppm: 9.80 (2H, s, imine CH), 9.37 (2H, d, *J* = 9.4 Hz, ArH), 8.88 (2H, d, *J* = 8.1 Hz, ArH), 8.55 – 8.13 (14H, br, ArH), 7.71 (4H, s, ArH) (Figure A-37).

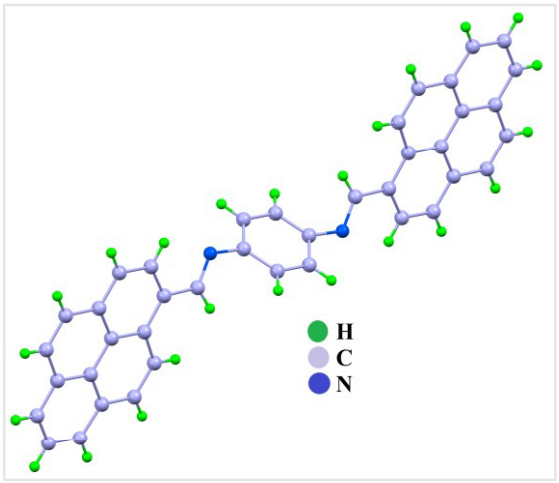

3B.2.4 Synthesis of (1*E*,2*E*)-1,2-bis(pyren-1-ylmethylene)hydrazine (L6a)

Hydrazine hydrate (0.121 mL, 2.5 mmol) was added dropwise to ethanolic solution of 1-pyrenecarboxaldehyde (1.15 g, 5 mmol), then catalytic amount of TFA (2-3 drops) was added to this solution. The mixture was refluxed for 24 hours. Pale yellow precipitate was removed by filtration and recrystallized from chloroform. Yield: 52%; Melting point: >300 ˚C; IR (cm^{-1}): 3099 (w), 2360 (w), 1913 (w), 1597 (s), 1388 (w), 1311 (w), 1242 (m), 1804 (m), 887 (w), 817 (s), 748 (m), 709 (m), 678 (w), 509 (m) (Figure A-38); ^{1}H NMR (400 MHz, DMSO-d_6) δ ppm: 9.94 (2H, s, imine CH), 9.30 (2H, d, *J* = 9.2 Hz, ArH), 8.86 (2H, d, *J* = 8.0 Hz, ArH), 8.53 – 8.42 (6H, m, ArH), 8.41 – 8.28 (6H, m, ArH), 8.19 (2H, t, *J* = 7.7 Hz, ArH) (Figure A-39); ^{13}C NMR (100 MHz, DMSO-d_6) δ ppm: 150.89, 133.19, 131.28, 130.65, 129.93, 129.84, 129.44, 128.55, 127.73, 127.51, 127.05, 126.69, 125.38, 124.99, 124.74, 124.46, 123.89 (Figure A-40).

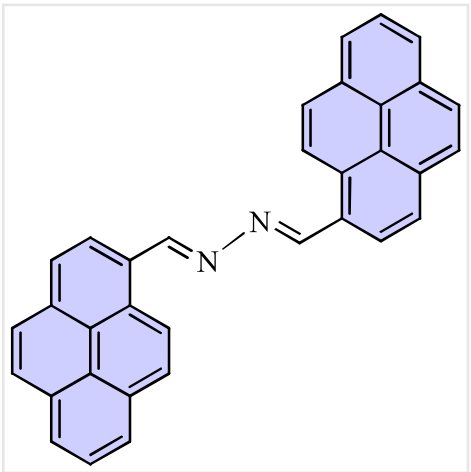

3B.2.5 Synthesis of (1*E*,1'*E*)-*N*,*N*'-(ethane-1,2-diyl)bis(1-(pyren-1-yl)methanimine) (L7a)

Ethylene diamine (0.167 mL, 2.5 mmol) was added dropwise to ethanolic solution of 1-pyrenecarboxaldehyde (1.15 g, 5 mmol) then catalytic amount of TFA (2-3 drops) was added

Table 3B.1: Crystallographic data of **L5a**

Parameters	**L5a**
Chemical formula	$C_{40}H_{24}N_2$
Formula weight	532.61
Temperature (K)	293(2)
Wavelength (Å)	0.71073
Crystal system	Orthorhombic
Space group	*Pbca*
a (Å)	12.1071(5)
b (Å)	14.3548(6)
c (Å)	15.1617(6)
α (°)	90
β (°)	90
γ (°)	90
Z	4
Volume (Å^3)	2635.03(19)
Density (g/cm^3)	1.343
μ (mm^{-1})	0.078
Theta range	2.578° to 28.289°
F(000)	1166
Reflections collected	39914
Independent reflections	3251
Reflections with I >2σ(I)	1705
R_{int}	0.0969
Number of parameters	1990
GO F on F^2	1.103
Final R_1[a]/wR_2[b] (I >2σ(I))	0.0768
Largest diff. peak and hole (eÅ^{-3})	0.305 & -0.505

[a] $R_1 = \sum||F_o| - |F_c||/\sum|F_o|$. [b] $wR_2 = [\sum w(F_o^2 - F_c^2)^2/\sum w(F_o^2)^2]^{1/2}$, where $w = 1/[\sigma^2(F_o^2) + (aP)^2 + bP]$, $P = (F_o^2 + 2F_c^2)/3$

to this solution. The mixture was refluxed for 24 hours. Dark orange precipitate was removed by filtration and recrystallized from chloroform. Yield: 48%; Melting point: 225 - 226 °C; IR (cm^{-1}): 1627 (s), 1435 (w), 1242 (w), 1064 (w), 972 (w), 840 (s), 756 (m), 717 (m), 609 (m) (Figure A-41); ^{1}H NMR (400 MHz, DMSO-d_6) δ ppm: 9.48 (2H, s, imine CH), 9.11 (2H, d, *J* = 9.4 Hz, ArH), 8.57 (2H, d, *J* = 8.1 Hz, ArH), 8.37 – 8.15 (12H, m, ArH), 8.09 (2H, t, *J* = 7.6 Hz, ArH), 2.09 (4H, s, 2×CH_2) (Figure A-42).

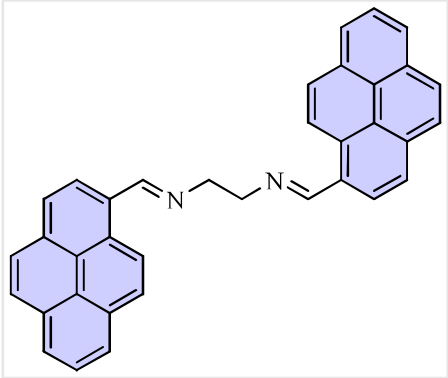

3B.2.6 Synthesis of (1*E*,1'*E*)-*N*,*N*'-(butane-1,4-diyl)bis(1-(pyren-1-yl)methanimine) (L8a)

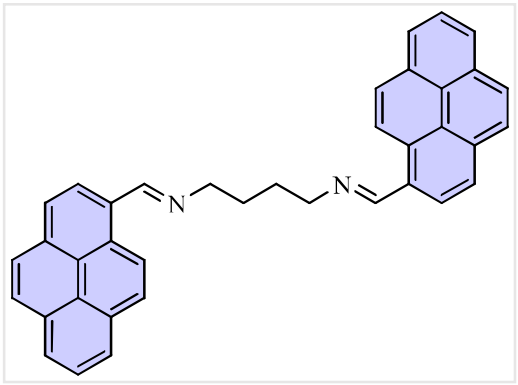

1,4-Diaminobutane (0.251 mL, 2.5 mmol) was added dropwise to ethanolic solution of 1-pyrenecarboxaldehyde (1.15 g, 5 mmol) then catalytic amount of TFA (2-3 drops) was added to this solution. The mixture was refluxed for 24 hours. Bright red precipitate was removed by filtration and recrystallized from chloroform. Yield: 54%; Melting point: >200 °C; IR (cm^{-1}): 3741 (w), 3039 (w), 2360 (w), 1743 (s), 1620(m), 1535 (w), 1458 (w), 1365 (w), 1234 (s), 1080 (s), 856 (s), 717 (m), 632 (m) (Figure A-43); ^{1}H NMR (400 MHz, DMSO-d_6) δ ppm: 9.45 (2H, s, imine CH), 9.12 (2H, d, J = 9.4 Hz, ArH), 8.58 (2H, d, J = 8.1 Hz, ArH), 8.39 – 8.19 (12H, m, ArH), 8.12 (2H, t, J = 7.6 Hz, ArH), 3.94 (4H, br, 2×CH_2), 1.95 (4H, br, 2×CH_2) (Figure A-44); HRMS: m/z calcd for $C_{38}H_{28}N_2$ $(M+H)^+$ = 513.2325, found 513.2302 (Figure A-45).

3B.2.7 Synthesis of (1*E*,1'*E*)-*N*,*N*'-(hexane-1,6-diyl)bis(1-(pyren-1-yl)methanimine) (L9a)

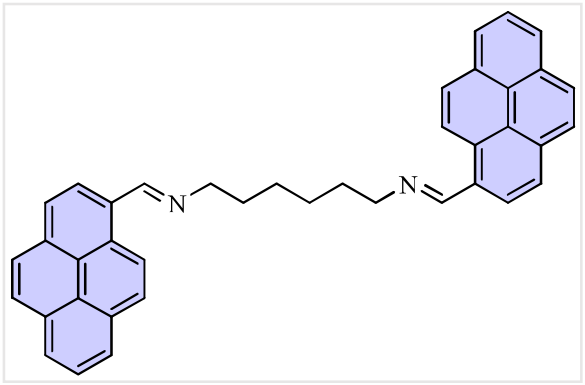

Hexamethylene diamine (0.346 mL, 2.5 mmol) was added dropwise to ethanolic solution of 1-pyrenecarboxaldehyde (1.15 g, 5 mmol) then catalytic amount of TFA (2-3 drops) was added to this solution. The mixture was refluxed for 24 hours. Light yellow precipitate was removed by filtration and recrystallized from chloroform. Yield: 65%; Melting point: 189 - 190 °C; IR (cm^{-1}): 3039 (w), 2360 (m), 1627 (m), 1308 (w), 1242 (w), 1804 (w), 1026 (w), 848(s), 748 (m), 678 (w) (Figure A-46); ^{1}H NMR (400 MHz, DMSO-d_6) δ ppm: 9.39 (2H, s, imine CH), 9.11 (2H, d, J = 9.4 Hz, ArH), 8.53 (2H, d, J = 8.1 Hz, ArH), 8.43 – 8.15 (12H, br, ArH), 8.11 (2H, t, J = 7.6 Hz, ArH), 3.84 (4H, br, 2×CH_2), 1.90 – 1.77 (4H, br, 2×CH_2), 1.64 – 1.52 (4H, br, 2×CH_2) (Figure A-47); ^{13}C NMR (100 MHz, DMSO-d_6) δ ppm: 160.17, 132.56, 131.25, 130.57, 129.57, 129.05, 129.01, 128.93, 127.84, 126.97, 126.86, 126.46, 126.14, 125.43, 124.48, 124.22, 123.47, 61.86, 31.19, 27.26

(Figure A-48); HRMS: m/z calcd for $C_{40}H_{32}N_2$ $(M+H)^+$ = 541.2638, found 541.2615 (Figure A-49).

3B.3 Results and Discussion

3B.3.1 Crystal Structure Analysis of L5a

The compound **L5a** is crystallized in *P*bca space group and half of the molecule is present in asymmetric unit. Crystal structure analysis revealed that the geometry attained by the molecule of **L5a** is such that the pyrene plane inclined by an angle of 64.57° with respect to the phenylene plane, while relatively negligible distortion is present in the imine functional groups of the molecule in which imine carbon has attained the trigonal planar geometry (Figure 3B.2a). Packing of the **L5a** molecules is via non-covalent interactions which include aromatic π•••π, aromatic C-H•••π and very weak C-H•••N hydrogen bonding interactions (Figure 3B.2b). The benzene ring in each molecule of **L5a**, interacts with two pyrene group of neighbouring **L5a**

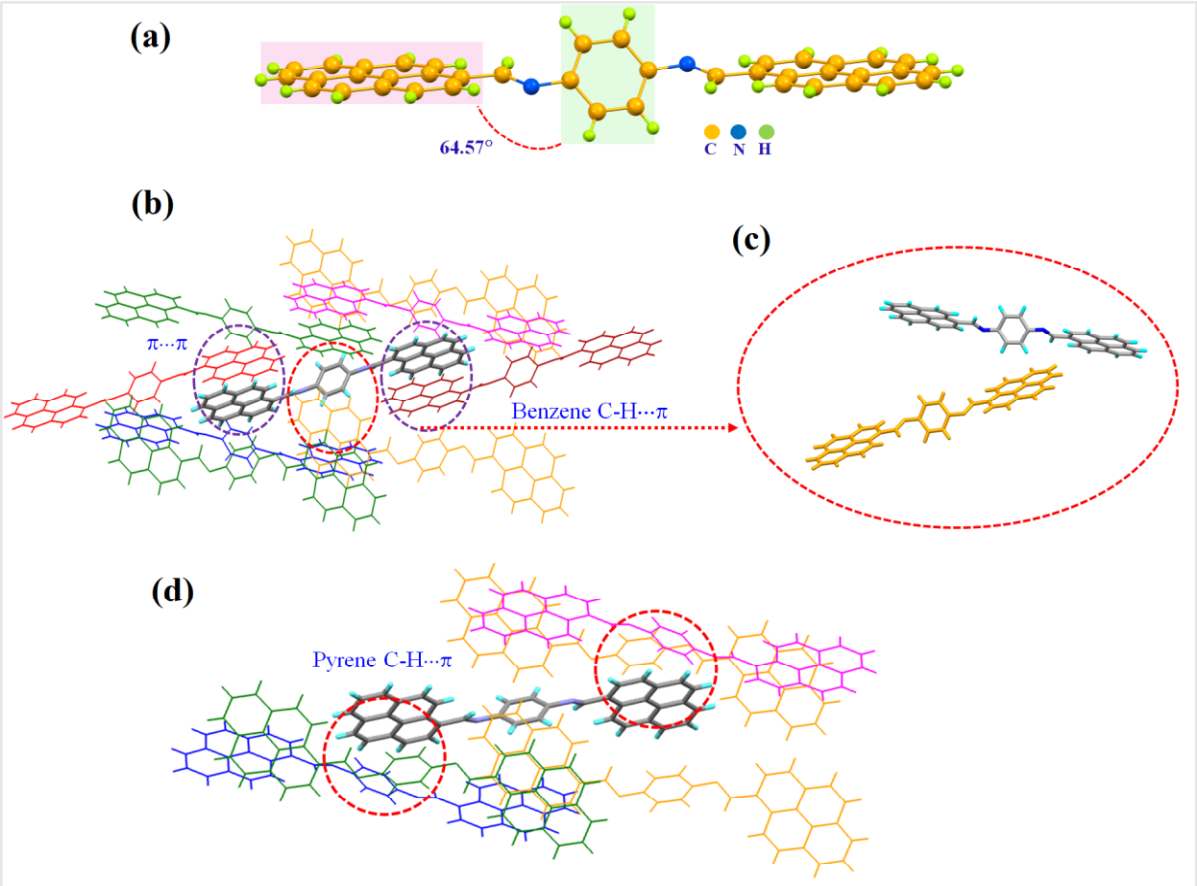

Figure 3B.2: Illustrations of crystal structure of **L5a**: (a) Molecular geometry of **L5a**; (b) Non-covalent interactions present between the molecules of **L5a**; (c) Benzene C-H•••π interactions between two **L5a** molecules; (d) Pyrene C-H•••π interactions between two **L5a** molecules

molecules via aromatic C-H•••π interactions (Figure 3B.2c). The pyrene group of each **L5a** also interacts with another pyrene ring via parallel aromatic π•••π interactions (Figure 3B.2b). Apart from these interactions, the C-H of pyrene also shows C-H•••π interaction with benzene ring of another **L5a** molecule (Figure 3B.2d). All these non-covalent interactions between the molecules of **L5a** resulted in the 3D packing of the molecules. Although the molecules of **L5a** are not overlapping over one another, neighbouring **L5a** molecules are packed in such a way that the pyrene groups of each molecule are stacked above pyrene groups of another molecule in a parallel manner. Presence of phenylene group in the spacer and its C-H•••π interaction with the pyrene of adjacent molecule results in disruption of uniform π-π stacking of pyrene groups (Figure 3B.3).

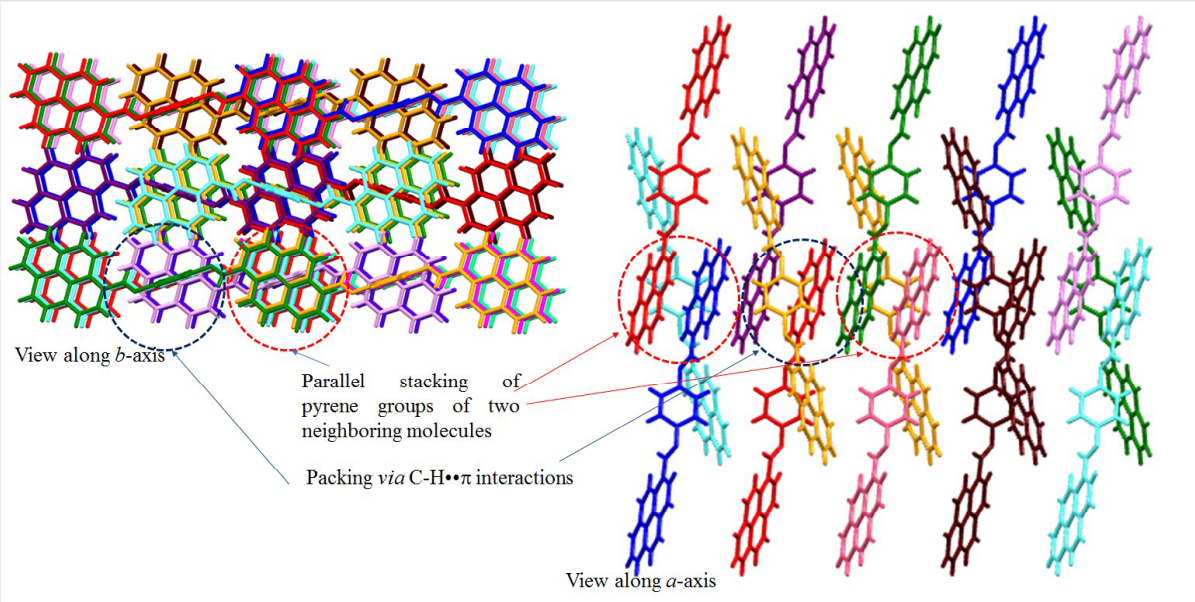

Figure 3B.3: Illustrations of crystal structure of **L5a**: Packing of **L5a** molecules in three dimensions

3B.3.2 UV-Visible Absorption Studies

UV-Visible absorption spectra for compounds **L5a** to **L9a** were recorded in *N*,*N*-dimethylformamide (DMF) and also in solid state by mixing the compounds with $BaSO_4$. UV-Visible spectra of **L7a**-**L9a** in DMF shows similar pattern as these compounds have alkylene groups as spacers and the peak maxima observed are mainly due to the same chromophore i.e the pyrene unit connected to imine group. In **L5a** and **L6a**, presence of hydrazine and phenylene spacer groups resulted in extended conjugation in the molecule and the UV-visible spectra in DMF showed red shift of the peak positions. For all the compounds, the peak at

around 290 nm corresponds to $\pi \rightarrow \pi^*$ transition due to aromatic pyrene moiety, while the peaks in the range 360 nm – 420 nm are due to $n \rightarrow \pi^*$ transitions (Figure 3B.4).

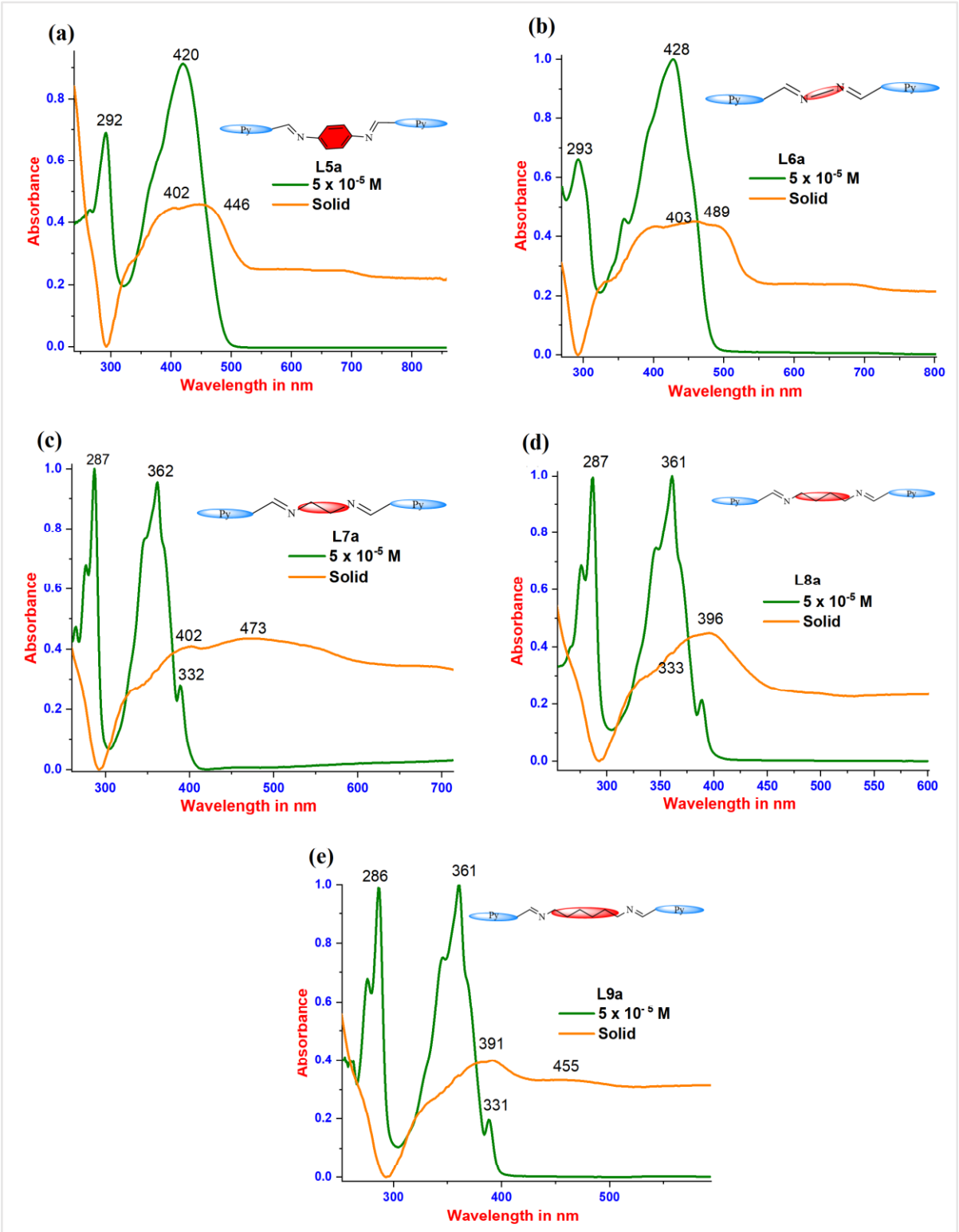

Figure 3B.4: UV-Visible spectra in DMF and solid-state (in $BaSO_4$): (a) **L5a**; (b) **L6a**; (c) **L7a**; (d) **L8a**; (e) **L9a**

An important feature that is common to all the compounds is the red shift of the peaks in solid state spectra when compared to that of the spectra taken in DMF. In DMF solution, **L5a** and **L6a** showed peak maxima at 420 nm and 428 nm, respectively which are red shifted to 447 nm and 489 nm in solid-state (Figure 3B.4a and 4b). For **L7a**, **L8a**, and **L9a**, the peaks observed at 362 nm, 361 nm and 389 nm in solution state are shifted to 473 nm, 396 nm, and 455 nm, respectively, in the solid state (Figure 3B.4c, 4d and 4e). All these observations indicate that as the concentration of the compounds increases and reaches a maximum (solid state), the supramolecular arrangement of the molecules results in the formation of J-aggregates. Crystal structure analysis of **L5a** also shows that the molecules are stacked in off-set manner, which closely resembles the J-aggregates. As the crystal structures of the other compounds could not be obtained, a hint can be obtained from the UV-visible spectra that the molecules might have offset or head-to-tail type of packing in the solid state.

3B.3.3 Aggregation caused quenching in L5a and L6a and Aggregation induced emission in L7a-L9a

Emission spectra of **L5a**-**L9a** were recorded in DMF at varied concentrations. Compounds **L5a** and **L6a** behaved in a different manner as compared to the compounds **L7a**-**L9a**. PL spectra of **L5a** and **L6a** showed intense emission peaks in the range 450-550 nm at low concentrations, however, on increasing their concentrations quenching was observed (Figure 3B.5). The solid-state PL spectra did not show any emission for these two compounds. Compounds **L7a**-**L9a** showed opposite behaviour, which is enhanced emission, when increasing concentration and

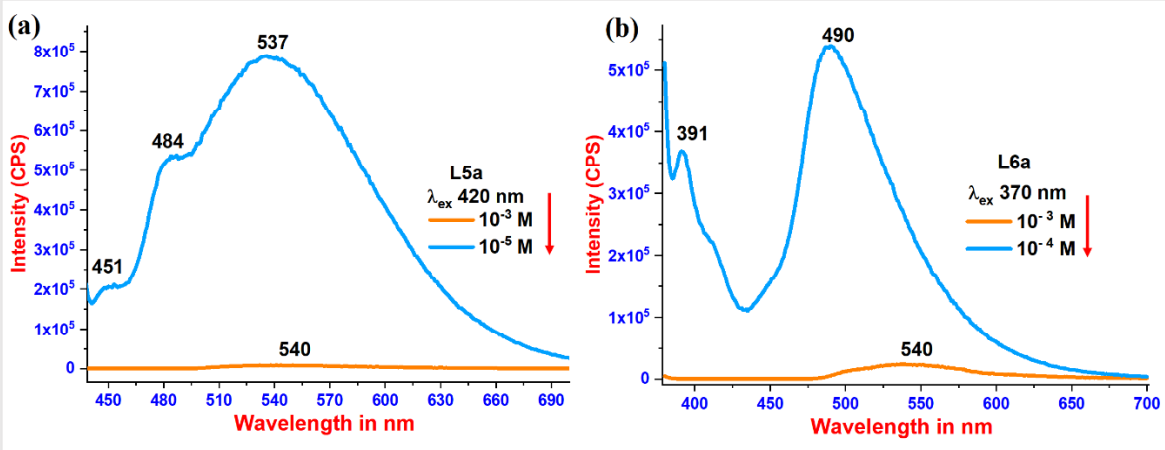

Figure 3B.5: PL spectra of (a) **L5a** (excitation wavelength 420 nm) and (b) **L6a** (excitation wavelength 370 nm) in DMF at different concentrations (slit width 10 nm)

also in the solid-state PL spectra. On increasing the concentration from 1×10^{-4} M to 1×10^{-3} M and finally in solid state of the compounds **L7a**-**L9a**, the emission maxima (λ_{max}) shifted to the higher wavelength region. Bathochromic shift observed for the compounds **L7a**, **L8a** and **L9a** are 79 nm, 66 nm and 29 nm, respectively (Figure 3B.6). The extent of red shift of peak positions indicates the formation of some non-covalently aggregated chromophore species.

Emission spectra of the compounds **L7a**-**L9a** were recorded in different ratio of THF-water solvent mixture. The compounds **L7a**-**L9a** are soluble in THF and addition of water will result in the formation of aggregates. The compounds **L8a** and **L9a** behaved in similar manner and both showed maximum intensity at the solvent ratio of 30:70 (THF: water) (Figure 3B.7), while compound **L7a** showed the maximum intensity at the solvent ratio of 60:40 (THF: water). The aggregates results in restriction of intramolecular rotations/vibrations and also may effectively reduce the aromatic stacking which may effect in excimer formation. Longer alkylene spacer in **L8a** and **L9a** induces more flexibility in the molecule, so more extent of aggregation is required for effectively reducing the intramolecular rotations and vibrations. Hence maximum intensity appears for higher water fraction compared to that in **L7a**, where lower water fraction results in high intensity (Scheme 3B.2).

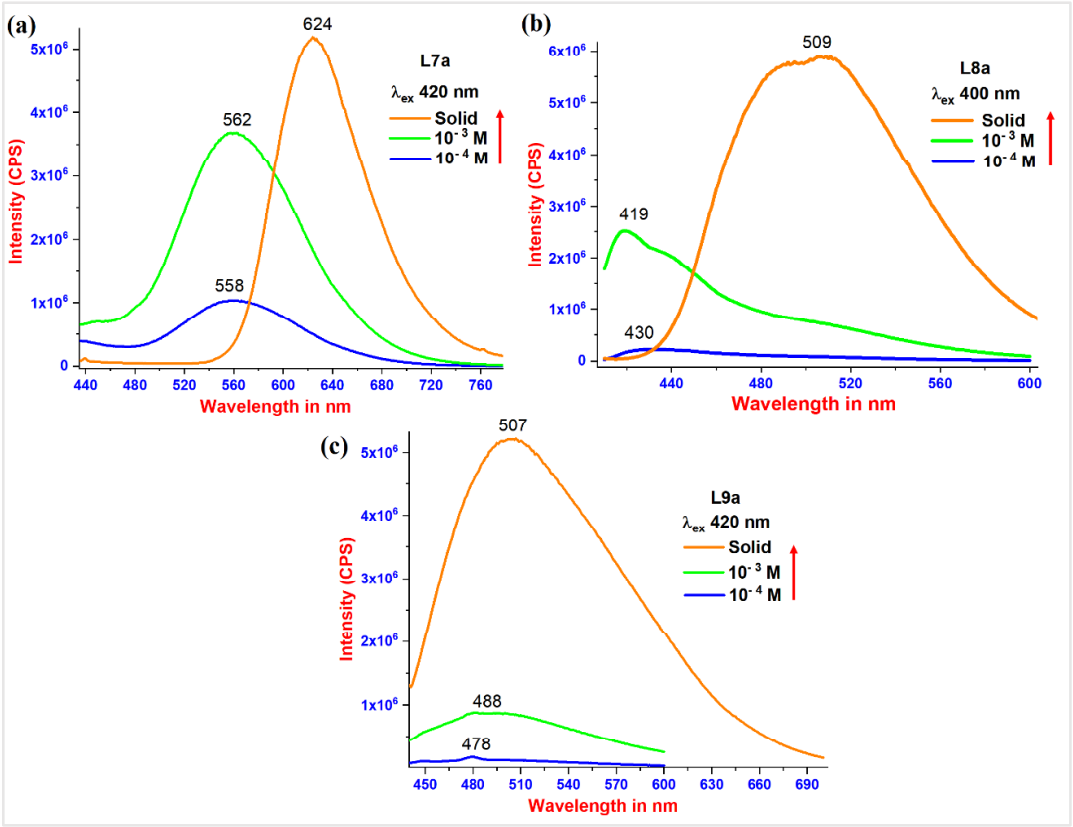

Figure 3B.6: PL spectra of (a) **L7a** (excitation wavelength 420 nm), (b) **L8a** (excitation wavelength 400 nm) and (c) **L9a** (excitation wavelength 420 nm) in DMF at different concentrations and in solid state

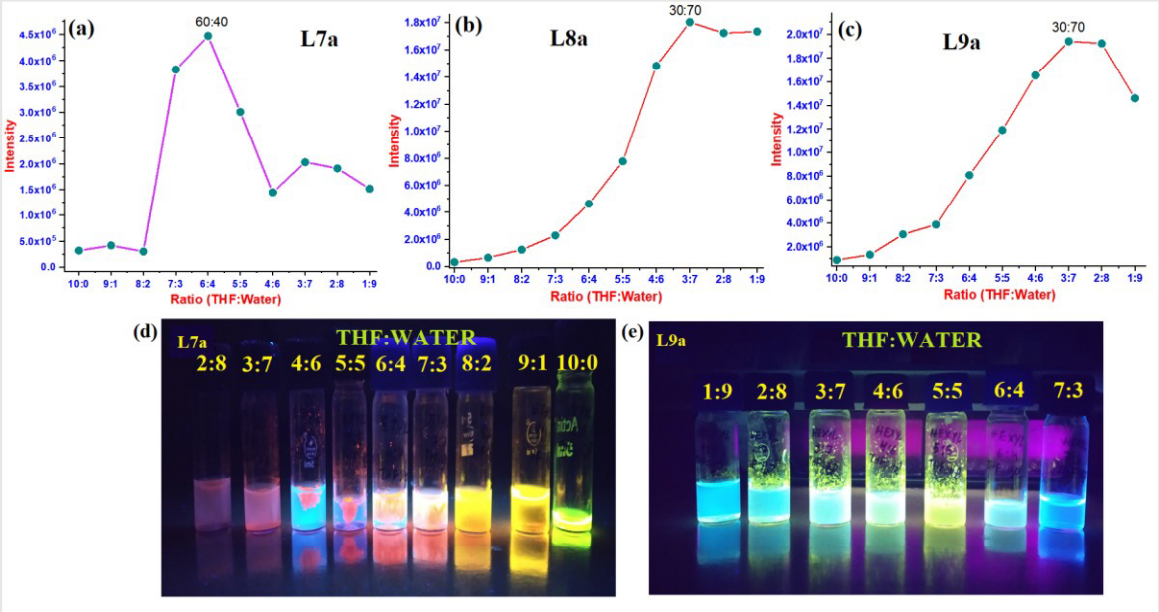

Figure 3B.7: Aggregation induced emission in THF: Water

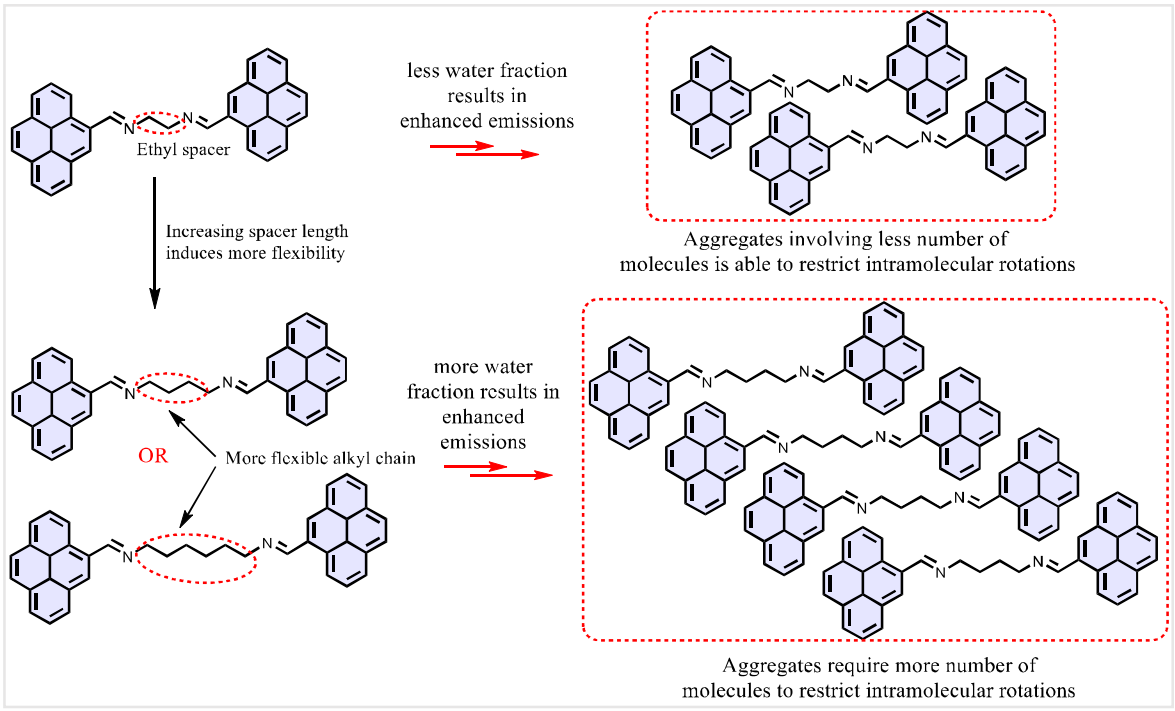

Scheme 3B.2: Length of alkyl spacer and its effect on aggregate concentration for maximum AIE

3B.3.4 Correlating the emission behaviour of L5a with its crystal structure and rationalizing the photophysical properties of L6a-L9a

Photoactive pyrene chromophore is faintly blue-emissive in lower concentration due to the presence of conjugation. Pyrene groups and phenylene spacer in **L5a** resulted in aromatic non-covalent interactions and has made the molecule locked into head-to-tail type of arrangement which is evident from its crystal structure analysis. In concentrated solutions of **L5a**, the

supramolecular arrangement of the molecules may be in a similar manner as that of the solid-state arrangement, where π-π stacking of pyrene rings might have occurred. Although the head-to-tail type of arrangement is categorized as J-type aggregate and it is also hinted from UV-visible spectral data, but the parallel π-π stacking of pyrene rings might have resulted in excimer formation and in turn is the reason for ACQ in **L5a**. ACQ effect of **L5a** is minimized in lower concentration and emissions are observed for low concentration PL spectra of **L5a**.

In **L6a**, absence of any alkylene/phenylene spacer resulted in giving more rigidity to the molecule and the molecules of **L6a** will have less chance of attaining any other non-covalent interaction apart from π-π stacking of pyrene rings. High concentrated solutions of **L6a** and solid compound of **L6a** showed quenching phenomena, which might have happened due to excimer formation. A very dilute solution of **L6a** represents almost monomeric form of the molecules and hence showed structured emission bands at 391 nm and 490 nm in its PL spectrum. On increasing the concentration of **L6a**, peak positions of its PL spectrum are red-shifted to 540 nm along with negligible fluorescence (Scheme 3B.3a).

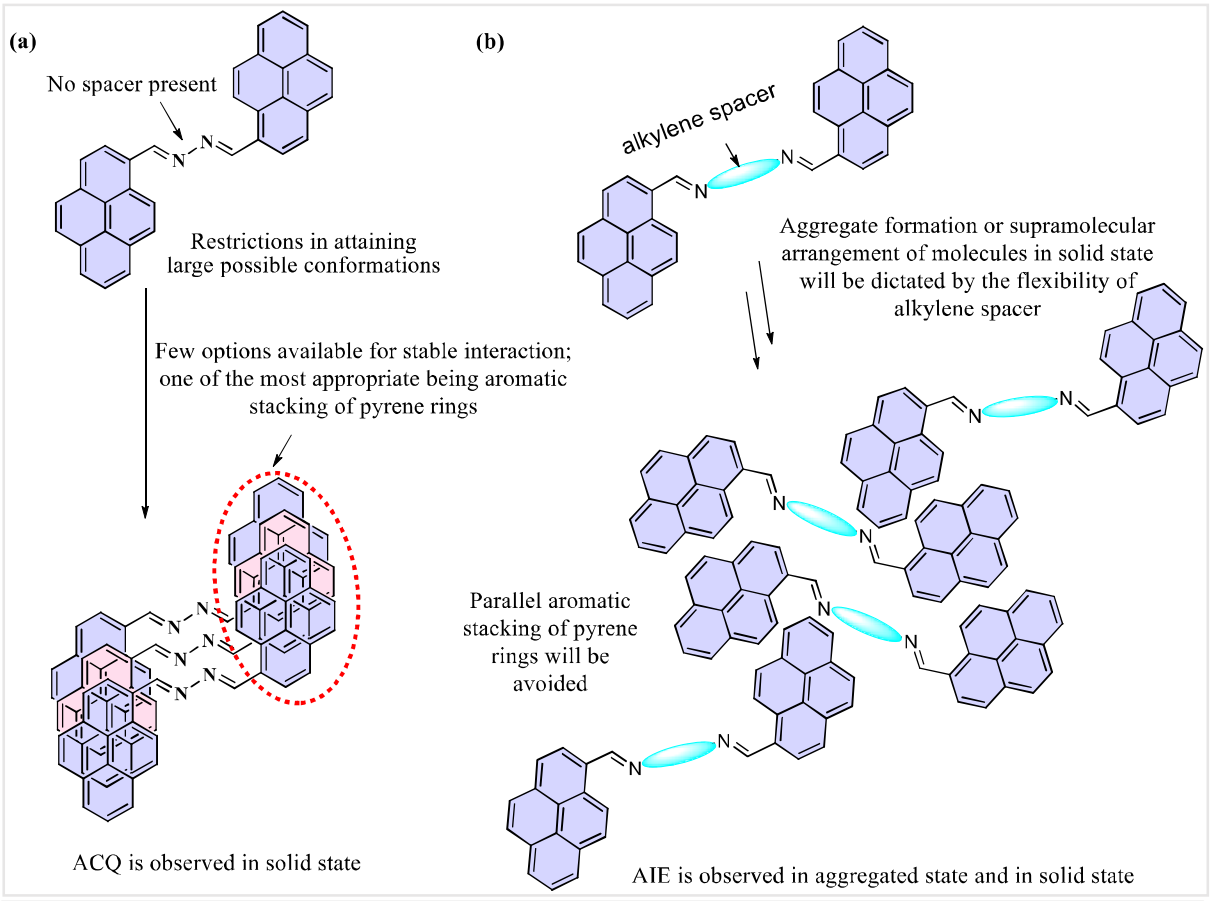

Scheme 3B.3:(a) ACQ observed on **L6a** due to stacking of aromatic rings; (b) AIE observed in **L7a**-**L9a** due to the presence of flexible alkyl chain in the spacer

In molecules **L7a**, **L8a** and **L9a**, presence of alkylene spacer, i.e., ethylene, butylene and hexylene group, respectively, has made the molecules flexible and non-planar. These compounds in dilute solutions show quenched emissions arising due to non-radiative decay resulting from intramolecular rotations and vibrations because of the flexibility induced by alkylene spacers. On increasing the concentrations, enhanced emission is observed in their PL spectra and the solid state PL also showed high emissions. AIE observed in **L7a**-**L9a** is attributed to the packing of molecules in such a way that their flexibility is lost, and the bathochromic shift of absorption spectra suggests head-to-tail type of aggregate formation and also an absence of any parallel π-π stacking of pyrene rings (Scheme 3B.3b).

3B.4 Conclusion

The photophysical properties of 1-pyrene substituted bis(pyrenyl)-di-imine Schiff bases were studied. The observed results were correlated with the structural behaviour of spacer group. Traditional pyrene excimer formation due to π-π stacking which is known as ACQ effect could be prevented by the nature of spacer group in aggregate or solid state. The flexible alkyl chain length in **L7a**, **L8a** and **L9a** was able to arrange the molecules in slipped arrangements so that the parallel aromatic π-π interactions was prevented and hence resulted in solid state emission. Presence of phenylene (**L5a**) and azine (**L6a**) in the spacer showed no emission due to π-π stacking (3.4 Å in **L5a**). In the solution state, **L5a** and **L6a** containing the phenylene and azine motifs resulted in very negligible emission as compared to alkylene containing **L7a**, **L8a**, and **L9a**. The head to tail arrangement in **L5a** leads J-aggregate in solution state. The intensity of emission shows an increase in aggregation for **L7a**, **L8a**, and **L9a** and the wavelength of the maximum intense peak also shows bathochromic shift indication J-type aggregate formation and head to tail or brick type stacking. The flexible alkylene spacer could be enough to solve the ACQ effect of pyrene for turn into AIEE.

3B.5 References

[1] Sęk D., Siwy M., Małecki J. G., Kotowicz S., Golba S., Nowak E. M., Sanetra J., Schab-Balcerzak E., *Spectrochim. Acta, Part A,* **2017**, 175, 168-176.

[2] (a) Le Bras L., Chaitou K., Aloïse S., Adamo C., Perrier A., *Phys. Chem. Chem. Phys.,* **2019**, 21(1), 46-56; (b) Jiang G., Li F., Kong X., Fan J., Song Y., Wang C.-K., Lin L., *J. Lumin.,* **2020**, 219, 116899.

[3] (a) Kawasaki T., Kamata T., Ushijima H., Murata S., Mizukami F., Fujii Y., Usui Y., *Mol. Cryst. Liq. Cryst. Sci. Technol., Sect. A,* **1996**, 286(1), 257-262; (b) Tang W., Xiang Y., Tong A., *J. Org. Chem.,* **2009**, 74(5), 2163-2166.

[4] (a) Mei J., Leung N. L., Kwok R. T., Lam J. W., Tang B. Z., *Chem. Rev.,* **2015**, 115(21), 11718-11940; (b) Gao M., Tang B. Z., *ACS Sens.,* **2017**, 2(10), 1382-1399; (c) Kelley T., Baude P., Gerlach C., Ender D., Muyres D. H., *Chem. Mater,* **2004**, 16, 4413.

[5] Luo J., Xie Z., Lam J. W. Y., Cheng L., Chen H., Qiu C., Kwok H. S., Zhan X., Liu Y., Zhu D., Tang B. Z., *Chem. Commun.,* **2001**, 2001(18), 1740-1741.

[6] Li K., Wang J., Li Y., Si Y., He J., Meng X., Hou H., Tang B. Z., *Sens. Actuators, B,* **2018**, 274, 654-661.

[7] Curtis M. D., Cao J., Kampf J. W., *J. Am. Chem. Soc.,* **2004**, 126(13), 4318-4328.

[8] Liu Y., Tao X., Wang F., Shi J., Sun J., Yu W., Ren Y., Zou D., Jiang M., *J. Phys. Chem. C,* **2007**, 111(17), 6544-6549.

[9] Alam P., Climent C., Alemany P., Laskar I. R., *J. Photochem. Photobiol., C,* **2019**, 41, 100317.

[10] Davis R., Saleesh Kumar N. S., Abraham S., Suresh C. H., Rath N. P., Tamaoki N., Das S., *J. Phys. Chem. C,* **2008**, 112(6), 2137-2146.

[11] Wang H., Liang Y., Xie H., Feng L., Lu H., Feng S., *J. Mater. Chem. C,* **2014**, 2(28), 5601-5606.

[12] Ma X., Sun R., Cheng J., Liu J., Gou F., Xiang H., Zhou X., *J. Chem. Educ.,* **2016**, 93(2), 345-350.

[13] Yamaguchi M., Ito S., Hirose A., Tanaka K., Chujo Y., *Mater. Chem. Front.,* **2017**, 1(8), 1573-1579.

[14] Li Q., Li Z., *Adv. Sci.,* **2017**, 4(7), 1600484.

[15] Huang Y., Xing J., Gong Q., Chen L.-C., Liu G., Yao C., Wang Z., Zhang H.-L., Chen Z., Zhang Q., *Nat. Commun.,* **2019**, 10(1), 169.

[16] Han T., Yan D., Wu Q., Song N., Zhang H., Wang D., *Chin. J. Chem .* **2021**, 39(3), 677-689.

[17] (a) Du X., Wang Z. Y., *Chem. Commun.,* **2011**, 47(14), 4276-4278; (b) Levitus M., Schmieder K., Ricks H., Shimizu K. D., Bunz U. H. F., Garcia-Garibay M. A., *J. Am. Chem. Soc.,* **2001**, 123(18), 4259-4265.

[18] Wu K. C., Ku P. J., Lin C. S., Shih H. T., Wu F. I., Huang M. J., Lin J. J., Chen I. C., Cheng C. H., *Adv. Funct. Mater.,* **2008**, 18(1), 67-75.

[19] Manandhar E., Wallace K. J., *Inorg. Chim. Acta,* **2012**, 381, 15-43.

[20] Berlman I. B., *J. Phys. Chem.,* **1970**, 74(16), 3085-3093.

[21] Moorthy J. N., Natarajan P., Venkatakrishnan P., Huang D.-F., Chow T. J., *Org. Lett.,* **2007**, 9(25), 5215-5218.

[22] Oyamada T., Uchiuzou H., Akiyama S., Oku Y., Shimoji N., Matsushige K., Sasabe H., Adachi C., *J. Appl. Phys.,* **2005**, 98(7), 074506.

[23] (a) Jadhav T., Dhokale B., Misra R., *J. Mater. Chem. C,* **2015**, 3(35), 9063-9068; (b) Jadhav T., Dhokale B., patil Y., Misra R., *RSC Adv.,* **2015**, 5(83), 68187-68191; (c) Misra R., Jadhav T., Dhokale B., Mobin S. M., *Chem. Commun.,* **2014**, 50(65), 9076-9078.

[24] Bains G. K., Kim S. H., Sorin E. J., Narayanaswami V., *Biochemistry,* **2012**, 51(31), 6207-6219.

[25] Dewar M. J., Dennington R. D., *J. Am. Chem. Soc.,* **1989**, 111(11), 3804-3808.

[26] Feng X., Xu Z., Hu Z., Qi C., Luo D., Zhao X., Mu Z., Redshaw C., Lam J. W. Y., Ma D., Tang B. Z., *J. Mater. Chem. C,* **2019**, 7(8), 2283-2290.

[27] Zhao Z., Chen S., Lam J. W. Y., Lu P., Zhong Y., Wong K. S., Kwok H. S., Tang B. Z., *Chem. Commun.,* **2010**, 46(13), 2221-2223.

[28] (a) Baig F., Kant R., Gupta V. K., Sarkar M., *RSC Adv.,* **2015**, 5(63), 51220-51232; (b) Das M., Baig F., Sarkar M., *RSC Adv.,* **2016**, 6(63), 57780-57792.

[29] Feng X., Hu J. Y., Redshaw C., Yamato T., *Chem. Eur. J.,* **2016**, 22(34), 11898-11916.

[30] Crawford A. Catalytic Borylation of CH Bonds: A Route to Photophysically Interesting Pyrene Derivatives. **2011**: Durham University.

[31] García R., Melle-Franco M., Mateo-Alonso A., *Chem. Commun.,* **2015**, 51(38), 8037-8040.

[32] (a) Kumar M., Dhir A., Bhalla V., Sharma R., Puri R. K., Mahajan R. K., *Analyst,* **2010**, 135(7), 1600-1605; (b) Braun D., Langendorf R., *J. Prakt. Chem.,* **1999**, 341(2), 128-137.

[33] Shellaiah M., Wu Y.-H., Singh A., Ramakrishnam Raju M. V., Lin H.-C., *J. Mater. Chem. A,* **2013**, 1(4), 1310-1318.

[34] Babgi B. A., Alzahrani A., *J. Fluoresc.,* **2016**, 26(4), 1415-1419.

[35] Espinosa A., Otón F., Martínez R., Tárraga A., Molina P., *J. Chem. Educ.,* **2013**, 90(8), 1057-1060.

[36] Martínez R., Espinosa A., Tárraga A., Molina P., *Org. Lett.,* **2005**, 7(26), 5869-5872.

[37] Gopalakrishnan D., Srinath S., Baskar B., Bhuvanesh N. S., Ganeshpandian M., *Appl. Organomet. Chem.,* **2019**, 33(3), e4756.

[38] Sheldrick G. M., *Acta Crystallogr., Sect. C: Struct. Chem.,* **2015**, 71(1), 3-8.